J|A|C|S
ARTICLES
Published on Web 06/14/2006

# Coverage Dependent Supramolecular Structures: $C_{60}$:ACA Monolayers on Ag(111)

Bo Xu,[†] Chenggang Tao,[‡] Ellen D. Williams,[‡] and Janice E. Reutt-Robey*,[†]

*Contribution from the Department of Chemistry and Biochemistry, Department of Physics, University of Maryland, College Park, Maryland 20742, USA*

Received January 12, 2006; E-mail: rrobey@umd.edu

***Abstract:*** The dependence of supramolecular structure on fractional molecular coverage has been investigated for acridine-9-carboxylic acid (ACA) and the $C_{60}$:ACA binary molecular system. The coverage-dependent phase diagram for ACA is first determined from room-temperature STM imaging. At low molecular coverages ($\theta < 0.4$ ML, ML = monolayer), ACA forms a 2-D gas phase. Ordered ACA structures appear with increasing coverage: first a chain structure composed of ACA molecules linked by consecutive O−H···N hydrogen bonds ($\theta > 0.4$ ML), then a dimer structure composed of ACA dimers linked by paired carboxyl-carboxyl hydrogen bonds ($\theta \approx 1.0$ ML). Structures of the $C_{60}$:ACA binary system depend on the coverage of predeposited ACA. At intermediate (0.4 ML $\sim$ 0.8 ML) ACA coverages, $C_{60}$ deposition results in a hexagonal cooperative structure with the $C_{60}$ periodicity nearly 3 times that of the normal $C_{60}$ 2-D packing of 1 nm and exists in enantiopure domains. At higher ACA coverages, a $C_{60}$ quasi-chain structure is formed in which parallel $C_{60}$ chains are spaced by ACA dimer domains. The mechanistic role of the initial ACA phase in the formation of $C_{60}$:ACA supramolecular structures is described. Chemically intuitive molecular packing models are presented based on the observed STM images.

## 1. Introduction

Molecular self-assembly systems offer great potential in the "bottom-up" approach to nanofabrication for device miniaturization and molecular electronics.[1−3] Extension of this concept to surfaces can yield novel structures which may find applications in molecular recognition, catalysis, and nonlinear optics.[4−7] Usually, three kinds of noncovalent interactions are most important in supramolecular self-assembly: dipole−dipole,[8] metal−ligand,[9] and hydrogen bonding interactions.[10−12] The resulting structures reflect the subtle balance between intermolecular and molecular−substrate interactions. Understanding the hierarchy of these interactions is essential for developing nanostructures with tailored properties.

Multicomponent systems offer the potential of a broader range of structure and property control.[12−19] In such cases, adlayer structures depend on the mixture of molecular components as well as their relative coverage. With a different choice of components or a subtle change in coverage, different supramolecular structures can be produced.[17−19] Efforts in supramolecular engineering have been guided by molecular-level considerations of how prescribed intermolecular couplings are mediated by the substrate atomic lattice. These efforts have generally avoided molecular components with a tendency toward polymorphism. In the present paper, however, we describe how the polymorphism of individual molecular components can be harnessed for the fabrication of binary supramolecular structures. In particular, we demonstrate how the properties of different single-component phases select pathways to binary supramolecular arrangements.

The ACA molecule (see Scheme 1), with an intrinsic dipole moment and two functional groups (carboxyl group and ring

[†] Department of Chemistry and Biochemistry.
[‡] Department of Physics.

(1) Hecht, S. *Angew. Chem., Int Ed.* **2003**, *42* (1), 24−26.
(2) Lehn, J. M. *Science* **2002**, *295* (5564), 2400−2403.
(3) Joachim, C.; Gimzewski, J. K.; Aviram, A. *Nature* **2000**, *408* (6812), 541−548.
(4) Verbiest, T.; Van Elshocht, S.; Kauranen, M.; Hellemans, L.; Snauwaert, J.; Nuckolls, C.; Katz, T. J.; Persoons, A. *Science* **1998**, *282* (5390), 913−915.
(5) Lorenzo, M. O.; Baddeley, C. J.; Muryn, C.; Raval, R. *Nature* **2000**, *404* (6776), 376−379.
(6) Mulligan, A.; Lane, I.; Rousseau, G. B. D.; Johnston, S. M.; Lennon, D.; Kadodwala, M. *Angew. Chem., Int. Ed.* **2005**, *44* (12), 1830−1833.
(7) Barth, J. V.; Costantini, G.; Kern, K. *Nature* **2005**, *437* (7059), 671−679.
(8) Yokoyama, T.; Yokoyama, S.; Kamikado, T.; Okuno, Y.; Mashiko, S. *Nature* **2001**, *413* (6856), 619−621.
(9) Dmitriev, A.; Spillmann, H.; Lin, N.; Barth, J. V.; Kern, K. *Angew. Chem., Int. Ed.* **2003**, *42* (23), 2670−2673.
(10) Barth, J. V.; Weckesser, J.; Cai, C. Z.; Gunter, P.; Burgi, L.; Jeandupeux, O.; Kern, K. *Angew. Chem., Int. Ed.* **2000**, *39* (7), 1230−1234.
(11) Keeling, D. L.; Oxtoby, N. S.; Wilson, C.; Humphry, M. J.; Champness, N. R.; Beton, P. H. *Nano Lett.* **2003**, *3* (1), 9−12.
(12) Theobald, J. A.; Oxtoby, N. S.; Phillips, M. A.; Champness, N. R.; Beton, P. H. *Nature* **2003**, *424* (6952), 1029−1031.
(13) Yoshimoto, S.; Higa, N.; Itaya, K. *J. Am. Chem. Soc.* **2004**, *126* (27), 8540−8545.
(14) Suto, K.; Yoshimoto, S.; Itayat, K. *J. Am. Chem. Soc.* **2003**, *125* (49), 14976−14977.
(15) Pan, G. B.; Liu, J. M.; Zhang, H. M.; Wan, L. J.; Zheng, Q. Y.; Bai, C. L. *Angew. Chem., Int. Ed.* **2003**, *42* (24), 2747−2751.
(16) Griessl, S. J. H.; Lackinger, M.; Jamitzky, F.; Markert, T.; Hietschold, M.; Heckl, W. A. *Langmuir* **2004**, *20* (21), 9403−9407.
(17) de Wild, M.; Berner, S.; Suzuki, H.; Yanagi, H.; Schlettwein, D.; Ivan, S.; Baratoff, A.; Guentherodt, H. J.; Jung, T. A. *ChemPhysChem* **2002**, *3* (10), 881−885.
(18) Bonifazi, D.; Spillmann, H.; Kiebele, A.; de Wild, M.; Seiler, P.; Cheng, F. Y.; Guntherodt, H. J.; Jung, T.; Diederich, F. *Angew. Chem., Int. Ed.* **2004**, *43* (36), 4759−4763.
(19) Stepanow, S.; Lingenfelder, M.; Dmitriev, A.; Spillmann, H.; Delvigne, E.; Lin, N.; Deng, X. B.; Cai, C. Z.; Barth, J. V.; Kern, K. *Nat. Mater.* **2004**, *3* (4), 229−233.

***Scheme 1.*** Molecular Components $C_{60}$ and Acridine-9-carboxylic Acid (ACA)

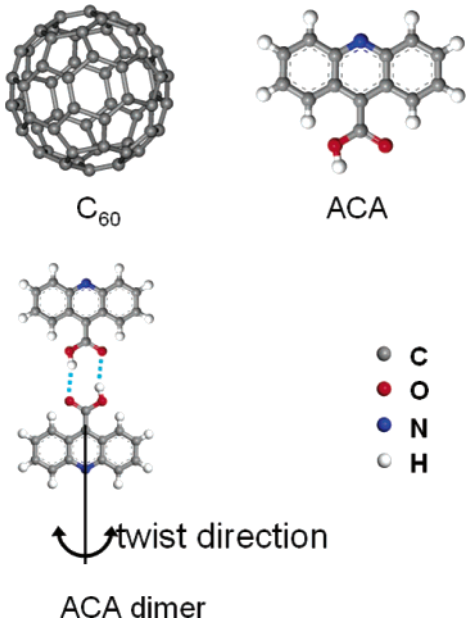


nitrogen atom), is a useful prototype for studying anisotropic intermolecular interactions.[20] Based upon the para-arrangement of its ring nitrogen atom and carboxyl group, ACA molecules can form two distinct intermolecular hydrogen bonds: in the head-to-tail H-bond arrangement, the ring N accepts the H-bond from the carboxyl tail of another ACA molecule, and in the tail-to-tail arrangement, two carboxyl groups associate ACA molecules into a dimer pair. The head-to-tail H-bond arrangement is found in dihydrate crystals of ACA,[21] as well as crystals of related molecules, such as nicotinic and isonicotinic acids.[22,23] Quantum chemistry calculations of gas-phase dimers of isonicotinic acid and ACA indicate that the head-to-tail hydrogen bonding motif is energetically preferred per hydrogen bond; however, the energy difference is quite small (40 meV).[24] With the additional influence from the Ag substrate, different ACA bonding configurations may occur.

It is known that $C_{60}$ molecules (see Scheme 1), codeposited with other molecules, can form a variety of surface structures differing from the hexagonally closed-packed structure usually formed when deposited alone on the surface.[12,17−19] Expanding upon the single-component phases, the binary $C_{60}$:ACA system provides further insight into the correlation between supramolecular structure and intermolecular interactions.

## 2. Experimental Materials

Our investigations were performed in an Omicron VT-STM system with a base pressure better than $5 \times 10^{-11}$ Torr. The procedures for Ag substrate preparation and vapor deposition of ACA and $C_{60}$ have been described previously.[25] All the STM data were taken at room temperature employing a constant current mode (typical tunneling current 50 pA, bias voltage −0.6 to −0.8 V). Molecular deposition through sublimation was monitored by a quartz microbalance and calibrated against STM images. The deposition rates for ACA and $C_{60}$ are 0.3 ML/min and 0.1 ML/min, respectively. Here, one monolayer (ML) of ACA is defined as one ACA molecule per eight Ag surface atoms, and one monolayer of $C_{60}$ is defined as one $C_{60}$ molecule per twelve Ag surface atoms.

## 3. Results

**3.1. 2-D Phases of ACA/Ag(111).** Our previous ACA/Ag(111) findings are extended with a more thorough mapping of the 2-D phase diagram and the discovery of a second ordered phase. A series of STM images of ACA molecules deposited on Ag is presented in Figure 1, for different coverages. Three phases emerge sequentially with increasing ACA coverage. When ACA coverage is low ($\theta \approx 0.3$ ML in Figure 1a), no molecule is directly resolved on the substrate except on very narrow terraces (widths < 6 nm) and along Ag step edges. Larger terraces are in fact occupied by mobile ACA molecules, which can be immobilized and imaged upon cooling the surface.[25] This low coverage phase of ACA on Ag is thus described as a two-dimensional gas phase.

Upon further ACA deposition to a coverage of 0.4 ML, the first ordered structure of ACA (ACA-α phase) appears. In Figure 1b ($\theta = 0.7$ ML), two large ACA islands (ordered structures) over 100 nm wide are imaged as dark regions. Frequent topographic jumps with identical heights (∼1 Å) are observed in the areas without the ACA ordered structure, indicating lifting and dropping of ACA molecules by the scanning tip. This is due to mobile ACA molecules in these areas. The 2-D gas phase and the ACA-α phase thus coexist on Ag(111) at this coverage.

A second ordered phase of ACA (ACA-$\beta$ phase) appears once the ACA coverage approaches 1 ML. In Figure 1c ($\theta \approx 1.0$ ML), three distinct structures are observed: two types of ordered domains with different brightnesses (topographic height) and narrow disordered regions separating the ordered domains. High-resolution STM images indicate the topographic lower ACA ordered domains (signed as ***A*** in Figure 1c) correspond to ACA-α phase domains mentioned above. These ACA-α phase domains decrease in area with the corresponding formation of brighter ACA-$\beta$ phase domains (signed as ***B*** in Figure 1c). A schematic diagram of the relationship between the ACA coverage and the fractional areas of different structures (with respect to the total surface area) is shown in Figure 1d.

Molecularly resolved STM images of the two different ordered phases are shown in Figure 2. Both phases are commensurate with the Ag(111) surface and indexed as (4 0, 2 4) and (5 0, 5 6) for the ACA-α phase and ACA-$\beta$ phase with respect to the Ag(111) surface, respectively. A unit cell for each of the ordered structures is superposed in the STM images. The structural parameters are summarized in Table 1. In the STM images (Figure 2a and 2b), each bright protrusion corresponds to one ACA molecule. The argument for this assignment was reported previously.[20] The shape and brightness difference of the protrusions can then be attributed to nonequivalent ACA orientations. It is clear that for the ACA-α phase there are two molecules in one unit cell, while there are four molecules (or two dimers) per unit cell for the ACA-$\beta$ phase. The molecular packing densities of these structures on the Ag surface are

(20) Xu, B.; Varughese, B.; Evans, D.; Reutt-Robey, J. *J. Phys. Chem. B* **2006**, *110* (3), 1271−1276.
(21) Patel, N. E.; Reutt-Robey, J. E. Submitted.
(22) Wright, W. B.; King, G. S. D. *Acta Crystallogr.* **1953**, *6* (4), 305−317.
(23) Takusagawa, F.; Shimada, A. *Acta Crystallogr., Sect. B* **1976**, *32* (Jun 15), 1925−1927.
(24) Evans, D.; Reutt-Robey, J. E. Unpublished.
(25) Xu, B.; Tao, C. G.; Cullen, W. G.; Reutt-Robey, J. E.; Williams, E. D. *Nano Lett.* **2005**, *5* (11), 2207−2211.

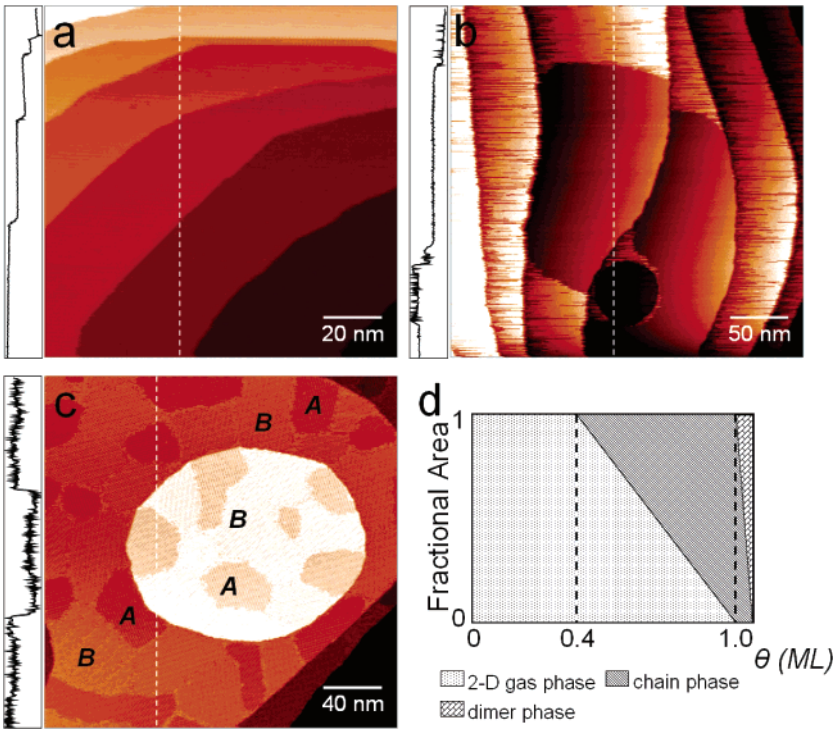


***Figure 1.*** Coverage dependent ACA adlayer structures (a, b, and c) and the schematic compositional phase diagram (d). STM images correspond to the samples with different ACA coverages, namely 0.3 ML (a), 0.7 ML (b), and 1.0 ML (c). Coexisting ordered phases are labeled ***A*** (chain phase) and ***B*** (dimer phase) in (c). A line profile is shown to the left for every STM image. The compositional phase diagram depicts the relationship between structure fractional area and ACA coverage on the Ag surface. Here one monolayer (ML) of ACA is defined as one ACA molecule per eight Ag surface atoms.

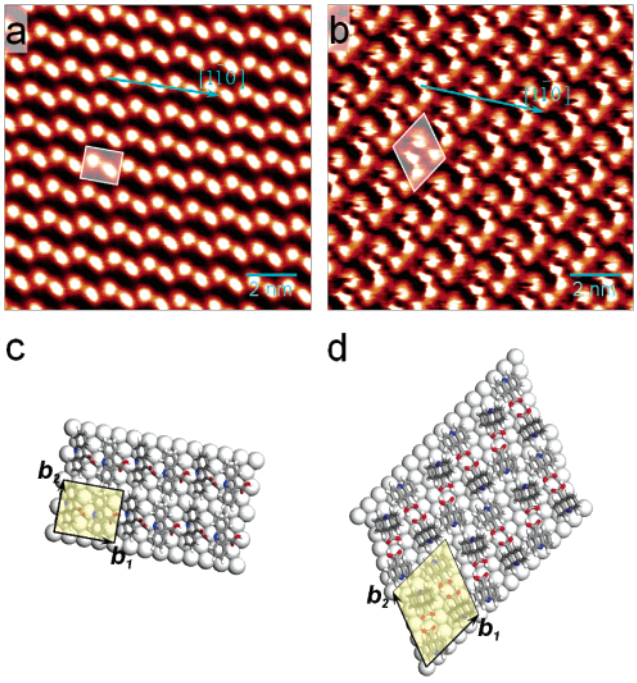


***Figure 2.*** Molecular resolved STM images of two distinct ACA ordered structures and proposed molecular packing models. (a, c) ACA-α ("chain") phase, local coverage $\theta = 1$ ML. (b, d) ACA-$\beta$ ("dimer") phase, local coverage $\theta = 16/15$ ML. The Ag [110] direction is indicated in the STM images. A set of primitive vectors ($\boldsymbol{b}_1$, $\boldsymbol{b}_2$) and a unit cell for the supramolecular structure are shown for each model.

distinct. If the surface density for the ACA-α phase is set as the reference unit (one ACA molecule per eight Ag surface atoms), the densities for the ACA-$\beta$ phase and 2-D gas phase are 16/15 and ca. 0.4 ML, respectively.

Previous XPS studies for 0.7 ML of ACA on Ag(111) indicate a predominant head-to-tail H-bonding configuration.[20] Based on the STM and XPS data, a molecular packing model for the ACA-α phase was proposed (Figure 2c). In this model, ACA molecules form head-to-tail H-bonds running along the [1$\bar{1}$0] direction of Ag(111). We define this ordered phase as a "chain" phase since the head-to-tail H-bonds link ACA molecules into parallel chains.

A molecular packing model is now proposed for the ACA-$\beta$ phase in Figure 2d. In this model, ACA molecules first organize into dimers that further assemble into ordered rows. We refer to this second ACA ordered phase as the "dimer" phase. To account for the high molecular packing density as well as the observed molecular shapes, the two ACA molecules are twisted with respect to each other while forming a dimer (see Scheme 1), and the two dimers inside of one unit cell are of opposite twist direction. This twist is consistent with quantum chemical calculation where two ACA molecules are not coplanar when forming a dimer.[24] We also noted there are six possible configurations (or domain types) for this dimer phase: a reflection along $\boldsymbol{b}_1$ in Figure 2d gives another configuration. Simple rotations of ±60° of the above two give the remaining four possible configurations. All these configurations are observed in experiments.

**3.2. Binary $C_{60}$ and ACA Films on Ag(111).** For ACA and $C_{60}$ deposition on Ag substrates, the resulting structures show a strong dependence on the deposition sequence, as demonstrated in Figure 3 for 0.4 ML of ACA and 0.4 ML of $C_{60}$. When $C_{60}$ molecules are deposited first, an ordered $2\sqrt{3} \times 2\sqrt{3}R30°$-$C_{60}$/Ag(111) phase forms even at a low coverage.[26]

(26) Altman, E. I.; Colton, R. J. *Phys. Rev. B* **1993**, *48* (24), 18244−18249.

***Table 1.*** Primitive Vector Parameters of the Adsorbed ACA and $C_{60}$ Supramolecular Structures with Respect to Ag(111)[a]

| Structure | ACA chain phase | ACA dimer phase | C60 closely packed phase | C60:ACA chiral phase | C60:ACA linear chain |
|---|---|---|---|---|---|
| Matrix | $\begin{pmatrix} 4 & 0 \\ 2 & 4 \end{pmatrix}$ | $\begin{pmatrix} 5 & 0 \\ 5 & 6 \end{pmatrix}$ | $\begin{pmatrix} 4 & 2 \\ -2 & 4 \end{pmatrix}$ | $\begin{pmatrix} 10 & 2 \\ -2 & 8 \end{pmatrix}$ for R, $\begin{pmatrix} 8 & -2 \\ 2 & 10 \end{pmatrix}$ for S | $\begin{pmatrix} 7 & 0 \\ 5 & 6 \end{pmatrix}$ |
| Molecular Packing Density | 1 ACA/8 Ag atoms | 1 ACA/7.5 Ag atoms | 1 $C_{60}$/12 Ag atoms | 1 ACA/14 Ag atoms or 1 $C_{60}$/84 Ag atoms | X |

[a] The primitive vectors for Ag(111) surface are along $[1\bar{1}0]$ and $[01\bar{1}]$ directions with the nearest neighbor distances.

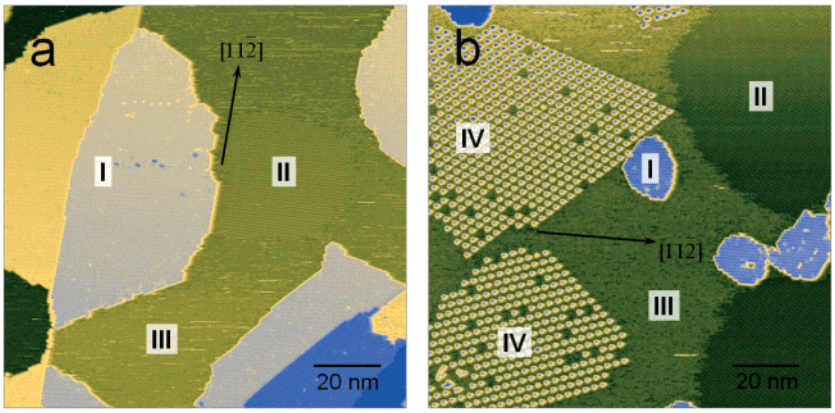


***Figure 3.*** STM images of $C_{60}$ and ACA supramolecular structures formed with reversed deposition sequences: (a) 0.4 ML of $C_{60}$ first, then 0.4 ML of ACA, (b) 0.4 ML of ACA first, then 0.4 ML of $C_{60}$. Labeled phases: I, $2\sqrt{3} \times 2\sqrt{3}R30°$-$C_{60}$/Ag(111); II, (4 0, 2 4)-ACA/Ag(111); III, 2-D ACA gas/Ag(111); and IV, $C_{60}$ and ACA intermixed phase. Ag [11$\bar{2}$] direction is indicated. The two IV domains in (b) are symmetric with respect to the Ag [11$\bar{2}$] direction.

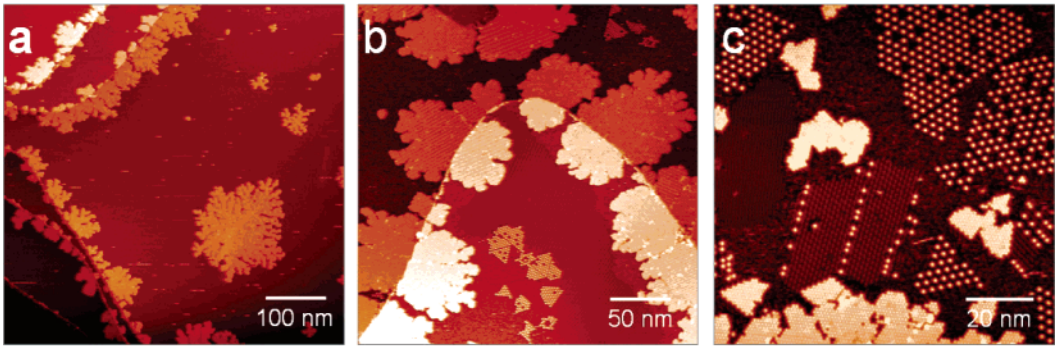


***Figure 4.*** Evolution of $C_{60}$:ACA supramolecular structures as a function of $C_{60}$ coverage. Initial ACA coverage is 0.3 ML. (a) 0.3 ML of $C_{60}$, (b) 0.55 ML of $C_{60}$, and (c) 0.65 ML of $C_{60}$ are added to the same surface.

If ACA molecules are subsequently deposited (Figure 3a), only phase-separated $C_{60}$- and ACA-domains appear. These single-component domains are structurally identical to those of the single component monolayers described above (labeled as I, II, and III in Figure 3a, respectively).[20,26] When the deposition sequence is reversed, a new supramolecular structure is observed (labeled as IV in Figure 3b). The highest features in phase IV are identified as $C_{60}$ molecules according to the shape and height. As previously described,[25] the domains of this new structure have distinct chiralities, and thus this structure is referred to as the $C_{60}$:ACA chiral phase.

Intermixed $C_{60}$:ACA structures depend on the coverage (phase) of the preexisting ACA film. Depositing $C_{60}$ in each of the three different ACA coverage regimes of Figure 1d results in different intermixed structures: for $\theta_{ACA} < 0.4$ ML, fullerene molecules do not immediately nucleate into the chiral phase with ACA. Instead, they form hexagonal closely packed islands of the $2\sqrt{3} \times 2\sqrt{3}R30°$ structure and increase the density of the surrounding ACA 2-D gas. The chiral phase is formed only when local $\theta_{ACA} > 0.4$ ML. In this coverage regime, fullerene molecules organize into both the closely packed $2\sqrt{3} \times 2\sqrt{3}R30°$ structures and the chiral structures. With suitable initial ACA coverage and varying $C_{60}$ coverage, we thus expect multiphase adlayer structures of ACA and $C_{60}$ on the Ag surface, as demonstrated in Figure 4. The initial ACA coverage (0.3 ML) is not sufficient for the formation of the chiral structure with a small subsequent $C_{60}$ deposition (Figure 4a). However, increasing $C_{60}$ adsorption compresses the residual ACA and increases the ACA local density, resulting in, first, $C_{60}$:ACA chiral structures (Figure 4b) and then linear arrangements of $C_{60}$ embedded between ACA-$\beta$ phase domains (Figure 4c). Because of the stronger interaction of $C_{60}$ molecules with Ag step edges, they tend to nucleate from those sites and grow into islands across Ag step edges. Details of these $C_{60}$:ACA intermixed structures are discussed in the following.

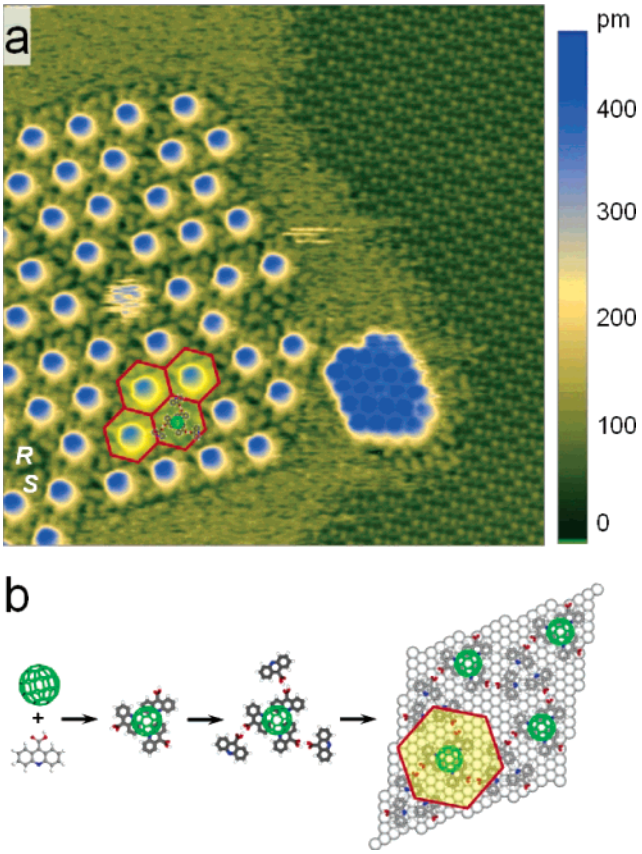


***Figure 5.*** STM image of a $C_{60}$:ACA intermixed *S* chiral domain (a) and proposed structural model (b). The coverages for ACA and $C_{60}$ are both 0.4 ML, with ACA deposited first. The hierarchical molecular assembly process is suggested in (b).

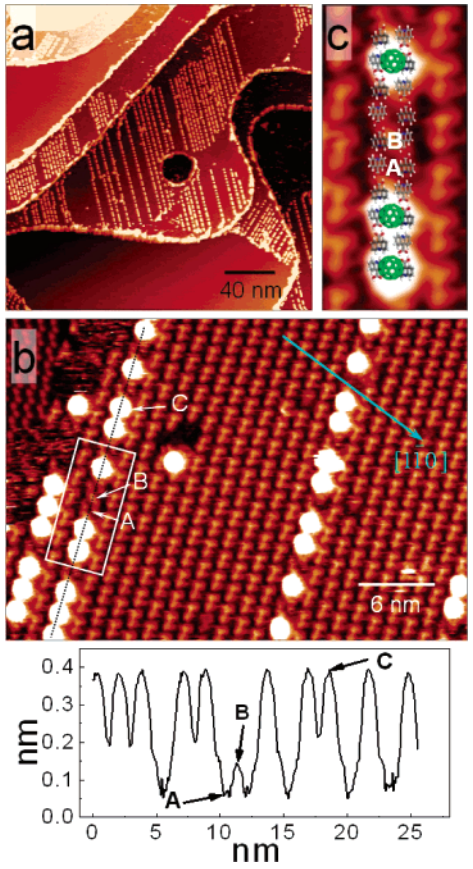


***Figure 6.*** Chainlike $C_{60}$:ACA supramolecular structure formed with $C_{60}$ deposition on predeposited ACA coverage (>0.8 ML). (a) A large scale STM image demonstrating parallel $C_{60}$ linear arrangement. (b) A higher resolution STM image showing the relative molecular positioning. A topographic profile is shown for the indicated line. A, B, C correspond to a $C_{60}$ vacancy, a local maximum between $C_{60}$ vacancies, and a $C_{60}$ molecule, respectively. (c) A suggested molecular packing model for the boxed area in (b).

As previously reported, the phase IV domains (Figure 3b) possess $2\sqrt{21} \times 2\sqrt{21}R \pm 10.9°$ or (10 2, −2 8) and (8−2, 2 10) structures in matrix notation with respect to the Ag(111) surface.[25] The structure is characterized by a 2.65 nm nearest-neighbor $C_{60}$ separation and an alternating pinwheel arrangement of ACA trimers. The mirror symmetry of IV domains with respect to the Ag [11$\bar{2}$] direction is a native result of the coexistence of two types of enantiopure domains with different chiralities.[5,27] Figure 5 presents a molecularly resolved STM image of one chiral domain (*S*) in coexistence with the 2-D ACA gas, the ACA chain phase domain, and the $2\sqrt{3} \times 2\sqrt{3}$ *R*30°-$C_{60}$ islands. Molecular organization along the $C_{60}$:ACA domain boundaries supports the proposed hierarchical molecular assembly model,[25] which is also presented in Figure 5b. The chiral domain is surrounded by the 2-D ACA molecular gas, indicating that chiral domain nucleation occurs within the 2-D ACA gas phase. This nucleation requires an appreciable ACA−$C_{60}$ interaction. Direct evidence for this interaction is found in the molecular structure in the immediate vicinity of the pure $C_{60}$ domain. Along the $C_{60}$ island border, ACA molecules are differently oriented from those inside of the pure ACA domain. A more detailed description of this ACA and $C_{60}$ intermixed chiral structure can be found in our previous report.[25]

A dramatically different $C_{60}$:ACA cooperative assembly structure is observed if the predeposited ACA coverage exceeds 0.8 ML. Subsequently adsorbing $C_{60}$ molecules induce the formation of the ACA-$\beta$ (dimer) domains and the linear arrangements of $C_{60}$ embedded between these ACA dimer domains, as demonstrated in Figure 6a. Chainlike $C_{60}$ arrangements have been previously observed with different coadsorbed molecular species.[18,19]

A higher resolved STM image of this chain structure is presented in Figure 6b. In this particular image, only one type of the two ACA dimers (in each unit cell) is imaged. Bias voltage dependent STM images indicate the invisibility of the other type of dimers is a tip effect, instead of a dimer structure other than the ACA dimer phase (see Supporting Information). As described above, the ACA dimer structure is commensurate with Ag(111). However, the unit cell is now (5 0, 1 6) in matrix notation with respect to Ag [1$\bar{1}$0] and [01$\bar{1}$] directions due to reflection operation compared with Figure 2b and 2d. The $C_{60}$ row is parallel to the Ag [15$\bar{6}$] direction and thus parallel to one of the ACA unit cell axes. The distance between neighboring $C_{60}$ molecules along the chain, 1.61 nm, is determined by the periodicity of the ACA dimer structure along this direction. Along the Ag[1$\bar{1}$0] direction, the effective width of the $C_{60}$ linear chain, as it spans neighboring ACA dimers in adjacent domains, is 7*a*, where *a* is the Ag lattice constant along Ag[1$\bar{1}$0]direction. This separation exceeds the 5***a*** periodicity of ACA dimer structure along Ag[1$\bar{1}$0]. A suggested $C_{60}$ linear chain structural

(27) Bohringer, M.; Schneider, W. D.; Berndt, R. *Angew. Chem., Int. Ed.* **2000**, *39* (4), 792−795.

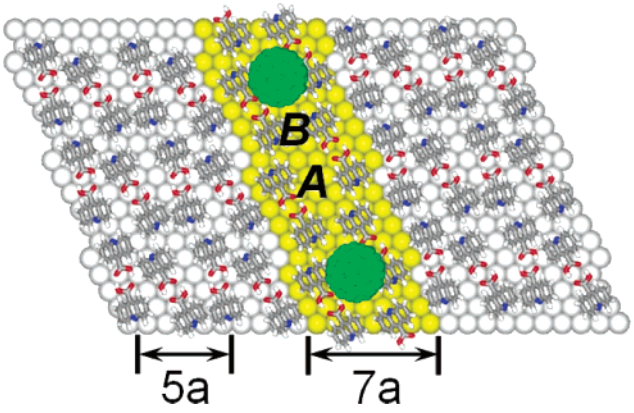


***Figure 7.*** Suggested molecular packing model for the chainlike $C_{60}$:ACA supramolecular structure based on the STM observations. The domain wall width is 7*a* along the Ag[1$\bar{1}$0] direction. Point ***A*** indicates a $C_{60}$ vacancy, and Point ***B*** indicates the local barrier between neighboring $C_{60}$ molecules.

model is shown in Figure 7. The width of this linear chain is emphasized by highlighting the underlying Ag atoms.

Additional molecular packing features of this $C_{60}$ linear arrangement are derived from the line profile indicated in the STM image of Figure 6b. The topographic maxima correspond to $C_{60}$, while the topographic minima correspond to $C_{60}$ vacancies. Finally, there is a local maximum between neighboring $C_{60}$ vacancies. The $C_{60}$ vacancies allow the ACA dimers beneath to be imaged: $C_{60}$ molecules sit between two rows of ACA dimers which are shifted with respect to each other along the Ag [15$\bar{6}$] direction by half of the dimer size. $C_{60}$ molecules are thus located in "valley sites" surrounded by ACA dimers. The green line in Figure 6b indicates a similar shift of the $C_{60}$ separated ACA domains along the Ag [15$\bar{6}$] direction.

To build these "valley sites" for $C_{60}$, the two rows of ACA dimer must have the same twist direction. Within the ACA dimer phase domain, the two rows of ACA dimer have the opposite twist direction. Consequently, these "valley sites" can only occur along the boundary between dimer domains. A molecular packing model for the $C_{60}$ chain phase structure is overlapped on top of the magnified STM image in Figure 6c, showing a good correspondence between the model and STM observation. Structural parameters for both mixed $C_{60}$:ACA phases are summarized in Table 1.

## 4. Discussion

In the following, we first discuss the origin and properties of the pure ACA phases and then turn to the $C_{60}$:ACA intermixed phases.

The extensive literature on phase transitions in two-dimensional systems provides a framework for interpreting the coverage-dependent ACA phase diagram.[28,29] A 2-D ACA molecular gas, exclusively observed for $\theta < 0.4$ ML, indicates repulsive ACA−ACA interactions in this low coverage regime. The onset of 2-D ACA islands (chain phase) reveals a crossover to attractive interactions between ACA molecules at the critical surface coverage of 0.4 ML. Finally, the emergence of a second ordered ACA phase around 1 ML signifies attractive ACA interactions of differing orientations.

These coverage-dependent phases can be reconciled with electrostatic interactions between chemisorbed ACAs. Free ACA molecules carry intrinsic multipole moments (especially a 1.7 D dipole directed just 40° from the aromatic plane and a 13.6 D·Å quadrupole ($Q_{zz}$ component) from Hartree−Fock calculation[24]). Upon chemisorption, charge transfer between molecular ACA and the Ag substrate introduces an interface dipole oriented normal to the surface place. Interactions between interface dipoles are necessarily repulsive, decreasing in magnitude with increasing coverage due to the depolarization effects. ACA molecules within the 2-D gas-phase adopt a flat-lying molecular orientation with respect to the surface plane.[25] For this orientation interactions between intrinsic dipoles are also repulsive. Evidently, in the low coverage regime, these repulsive interactions exceed the localized (short-range) H-bond attractive interaction.

The 0.4 ML ACA coverage signifies the critical point where attractive forces (such as short-range H-bonds) overcome dipole−dipole repulsion. Two ordered ACA phases, the ACA chain phase and dimer phase, are then observed with increasing coverage. The energy difference between these two ordered phases, or two H-bonding configurations, is small.[24] The lower density chain phase is energetically favored per molecule while the higher density dimer phase is energetically favored per surface area. Consequently, the chain phase emerges first and then the dimer phase with higher ACA coverage.

STM provides direct evidence that the formation of the dimer phase on large Ag terraces occurs via the consumption of the chain phase: domains of the chain phase ($\geq$100 nm width) shrink with the growth of the dimer phase. This indicates a first-order structural phase transition from the chain to dimer phase with increasing ACA coverage. Such molecular packing phase transitions have been observed in other 2-D systems. The driving force governing these transitions is ascribed to either packing constraints overcoming repulsive intermolecular forces at higher coverage[30] or preferred molecular adsorption sites and intricate intermolecular electrostatic interactions.[27]

From the phase diagram presented in Figure 1d, the fractional areas (with respect to the total surface area) for different ACA phases at the coverage $\theta = 0.7$ ML can be estimated using the lever rule:

$$\theta_g A_g + \theta_c A_c = \theta \qquad (1)$$

where the surface densities for the 2-D gas and chain phases are $\theta_g = 0.4$ ML and $\theta_c = 1.0$ ML, respectively, and the fractional area of the 2-D gas and ACA chain phase, $A_g$ and $A_c$, must sum to 1. We thus have $A_g = 0.5$ and $A_c = 0.5$. Half of the Ag surface is thus covered by ACA chain structure (containing 70% of the ACA molecules). This distribution is consistent with both STM and XPS results for 0.7 ML ACA/Ag(111).

One significant point is that, in order to achieve this high molecular packing density, a tilted molecular orientation of ACA on the surface is necessary. Fused ring aromatic molecules are generally expected to behave as $\pi$ donors to metallic substrates, which would favor a parallel orientation. However, with increased ACA packing density, the intermolecular interactions become more important and can stabilize the tilted molecular orientation. Previous studies involving N-heterocycles have also

(28) Einstein, T. *CRC Crit. Rev. Solid State Mater. Sci.* **1978**, *7* (3), 261−288.
(29) Naumovets, A. G. *Contemp. Phys.* **1989**, *30* (3), 187−201.
(30) Vidal, F.; Delvigne, E.; Stepanow, S.; Lin, N.; Barth, J. V.; Kern, K. *Journal of the American Chemical Society* **2005**, *127* (28), 10101−10106.

shown how the molecular packing density increases with a concomitant change in molecular orientation and N-substrate bonding.[31,32]

With the introduction of $C_{60}$, novel intermixed structures determined by the deposition order and componential molecular coverage are formed on Ag surfaces. The observed dependence on the deposition sequence reflects kinetic limitations in intermixed structure formation. At room temperature, $C_{60}$ molecules aggregate on the surface even at very low coverage due to strong attractive van der Waals interactions originating from the mutually induced polarization fluctuations on the molecules. In contrast, ACA molecules remain as a 2-D gas when $\theta < 0.4$ ML due to the lateral intermolecular repulsion. As a result, deposition of $C_{60}$ before ACA yields only phase-separated single component domains. However, a different scenario arises if ACA molecules are deposited first. When ACA coverage $\theta < 0.4$ ML, incoming $C_{60}$ molecules adsorb directly on the substrate and aggregate into small $C_{60}$ islands. This process shrinks the ACA 2-D gas phase area and effectively increases the ACA local density. The onset of the ACA chain phase reveals that the ACA 2-D gas has reached a local critical coverage, 0.4 ML. Continued $C_{60}$ deposition produces the $C_{60}$:ACA chiral phase: a $C_{60}$ molecule has greater possibility to induce a local ordering of an ACA trimer, with random selection of an *S* or *R* chirality. After the initial chirality creation event, subsequent assembly of ACA molecules is directed by hydrogen bonding interactions to maintain the defined chirality and registration with respect to the underlying Ag(111) lattice.

The chiral phases prove to be robust. Subsequently deposited $C_{60}$ molecules never occupy the ACA trimer of opposite chirality inside one domain even though the spacing is large enough to avoid steric $C_{60}-C_{60}$ repulsion. The initial symmetry breaking event evidently induces configurational differences between the two ACA trimers.[25]

The second intermixed $C_{60}$:ACA phase is closely related to the ACA-$\beta$ (dimer) phase. For the pure ACA film, the formation of the dimer phase requires a critical ACA coverage of 1 ML. The ACA dimer phase can also be induced by the addition of $C_{60}$ to ACA films at a lower ACA coverage. Site blocking by $C_{60}$ molecules increases the local density of ACA to 1.0 ML, introducing small domains of the ACA dimer phase. Individual $C_{60}$ molecules also interact directly with ACA dimers, leading to the formation of the $C_{60}$:ACA chain phase. In this phase, each $C_{60}$ molecule interacts with two ACA dimers which are shifted along the Ag [15$\bar{6}$] direction. This dimer shift occurs only when $C_{60}$ chains function as the wall between neighboring ACA dimer domains. The $C_{60}$ chains thus bridge two ACA domains which are shifted along the Ag [15$\bar{6}$] direction. Subsequent $C_{60}$ deposition does not produce new $C_{60}$ chains within ACA dimer domains. Instead, $C_{60}$ molecules fill vacancies in the existing $C_{60}$ chains or form chains along newly generated ACA dimer domain boundaries.

For both of the $C_{60}$:ACA cooperative structures, the nearest $C_{60}-C_{60}$ distances (2.65 nm for the $C_{60}$ chiral phase and 1.61 nm for the $C_{60}$ chain phase) are much larger than that in the $C_{60}$ hexagonal closely packed structure (1 nm), excluding structure stabilization by the $C_{60}-C_{60}$ cohesive energy. For the chiral phase, the underlying ACA structure (with *P*31*m* 2-D symmetry) differs from any pure ACA structure, indicating a substantial interaction between $C_{60}$ and ACA. Kinetic access to this structure is provided by the 2-D ACA molecular gas of critical density. For the $C_{60}$ chain phase, $C_{60}$ molecules sit between two ACA dimer domains glided with each other along the Ag [15$\bar{6}$]direction. The two rows of dimers directly under the $C_{60}$'s (same twist direction) have a different configurational arrangement compared with that in the ACA dimer phase (opposite twist direction of the two nonequivalent dimers in unit cell, Figure 2b). With the addiction of $C_{60}$, one row of dimers shifts with respect to the other with corresponding conformational change and produces valley sites for $C_{60}$ location. Again, the $C_{60}-$ACA interactions guide the structure: local interaction between $C_{60}$ and its adjacent ACA dimer influences the electronic and configurational structure of the nearest-neighbor ACA dimer. Propagation of these local changes in ACA dimer affects surrounding molecular organization and induces long-range interactions between fullerene molecules.[18,33] The row of fullerene molecules between neighboring ACA dimer domains evidently minimizes the structure free energy.

## 5. Conclusion

A coverage-dependent phase evolution is observed for ACA monolayer structures and can be qualitatively related to the electrostatic interactions among ACA molecules. The ACA molecules are presented in a 2-D gas phase, a chain phase, and a dimer phase with increasing molecular packing density. Based upon the room temperature observations, a fractional area vs coverage phase diagram for ACA/Ag(111) can be constructed. The ACA and $C_{60}$ coadsorbed systems show strong dependence on the deposition sequence, as well as the component coverage. Upon changing the initial ACA coverage, two distinct $C_{60}$:ACA cooperative structures are formed: the chiral intermixed structure, and the chainlike $C_{60}$ structure. The chiral $C_{60}$:ACA structure is based upon a critical local coverage of 0.4 ML of ACA, and the chain $C_{60}$:ACA structure is related to the ACA dimer phase. The arrangement of the fullerene molecules can thus be controlled by the coverage dependent predeposited ACA structures. These intermixed structures represent the delicate balance between $C_{60}-$ACA$-$Ag(111) interactions. The molecular conformational motion within the underlying ACA layer also plays a crucial role in realizing these structures. Our observations demonstrate a feasible method to fabricate surface nanostructures with novel properties, such as chirality, and one-dimensional packing.

**Acknowledgment.** We thank Dr. William Cullen for invaluable technical support. This work has been supported by the National Science Foundation under the MRSEC Grant DMR-05-20471 and under CHE-01-36401.

**Supporting Information Available:** Bias dependent STM images of the ACA dimer phase. This material is available free of charge via the Internet at http://pubs.acs.org.

JA060227F

(31) Giergiel, J.; Wells, S.; Land, T. A.; Hemminger, J. C. *Surf. Sci.* **1991**, *255* (1−2), 31−40.
(32) Lee, J. G.; Ahner, J.; Yates, J. T. *J. Chem. Phys.* **2001**, *114* (3), 1414−1419.
(33) Spillmann, H.; Kiebele, A.; Stohr, M.; Jung, T. A.; Bonifazi, D.; Cheng, F. Y.; Diederich, F. *Adv. Mater.* **2006**, *18* (3), 275−279.